Supporting Information

Bifunctional fluorescent iron-doped carbon dot-based nanozyme for highly sensitive dual-mode cascade detection of D-galactose

Lei Wang [a], Weiping Liu [b], Dan Qiu [a], Xingju Li [a], Yawen Lin [a], Yan Zhao [a,c*]

[a] School of Science, Xihua University, Chengdu, 610039, China

[b] Department of Clinical laboratory, Wuhan Third Hospital, Tongren Hospital of Wuhan University, Wuhan, 430060, China

[c] Sichuan Provincial Engineering Research Center of Molecular Targeted Diagnostic & Therapeutic Drugs, Xihua University, Chengdu 610039, China

*Corresponding authors:

Dr. Yan Zhao, Email address: zhao518yan@163.com

Table of contents:

different time points.

Fig. S10. Effects of different potential interferents on D-Gal detection: (A) fluorescence intensity and (B) UV absorption.

Table S1. Comparison of the kinetic parameters of different peroxidase mimics.

Table S2. Comparison of analytical methods for the determination of D-Gal

Materials and apparatus

P-Phenylenediamine (PPD), Ferrous chloride ($FeCl_2$), o-phenylenediamine (OPD), N-aminoethyl ethanolamine (AEEA), H_2O_2, 3,3′,5,5′-tetramethylbenzidine (TMB), sodium acetate (NaAc), acetic acid (HAc), ascorbic acid (AA), uric acid (UA), histidine (His), isopropyl alcohol (IPA), catalase (CAT), superoxide dismutase (SOD), terephthalic acid (TA), and 5,5-dimethyl-1-pyrroline N-oxide (DMPO) were purchased from Macklin Biochemical Co., Ltd. (Shanghai, China). SA, SOX, isoleucine (Ile), aspartate (Asp), valine (Val), arginine (Arg), threonine (Thr), alanine (Ala), cysteine (Cys), tryptophan (Trp), alkaline phosphatase (ALP), thrombin (TB), xanthine oxidase (XOD), trypsin (TRY), and glucose were supplied by Sigma-Aldrich Chemical Co. (St. Louis, MO, USA). Urine samples from healthy donors and prostate cancer patients were obtained from Tongren Hospital of Wuhan University.

UV-Vis absorption spectra were collected on a Shimadzu UV-2700 spectrometer (Shimadzu, Japan). Fluorescence spectra measurements were carried out on a HORIBA FluoroMax-4 spectrofluorometer (HORIBA, Japan). Fluorescence lifetimes were recorded with an Edinburgh FLS1000 spectrofluorometer (Edinburgh, UK). Electron paramagnetic resonance (EPR) spectra were recorded using an MS-5000X spectrometer (Magnettech, Germany). Atomic force microscopy (AFM) images were obtained on a Dimension FastScan atomic force microscope (Bruker, Germany). X-ray photoelectron spectroscopy (XPS) measurements were carried out using an ESCALAB 250Xi instrument (Thermo Fisher Scientific, USA). Transmission electron microscopy (TEM) was performed on an FEI Talos F200X instrument (FEI, USA). X-ray

diffraction (XRD) measurements were conducted on a DX-2800 diffractometer (HAOYUAN, China). Fourier transform infrared spectroscopy (FT-IR) spectra were collected using a Nicolet iS10 Fourier transform spectrometer (Thermo Fisher Scientific, USA).

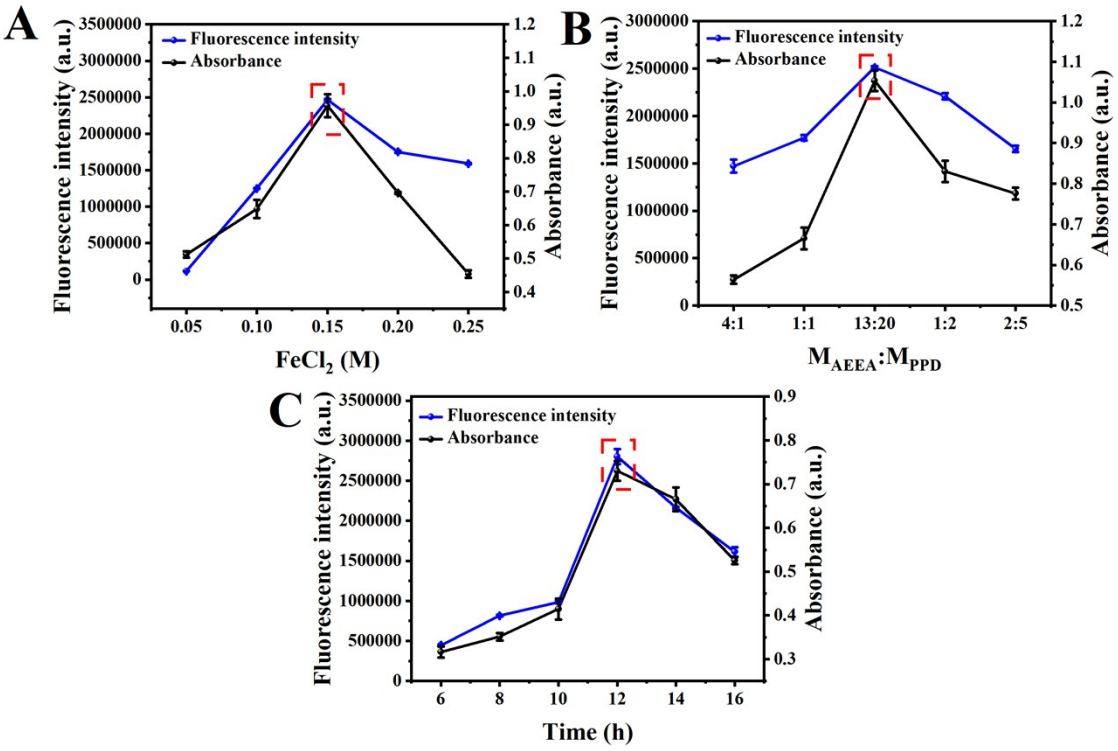

Fig. S1. (A) Effects of Fe^{2+} concentration, (B) mass ratio of AEEA to PPD, and (C) reaction time on the fluorescence intensity and absorbance of the Fe-CDs system.

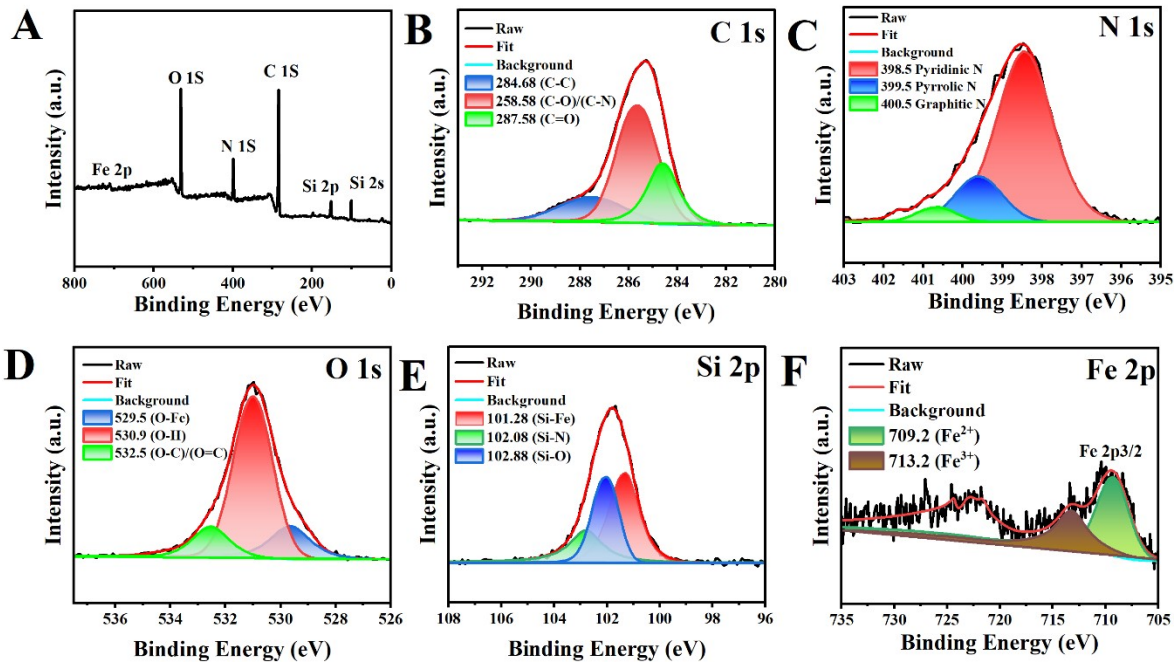

Fig. S2. (A) XPS survey spectrum of Fe-CDs, and high-resolution XPS spectra of (B) C 1s, (C) N 1s, (D) O 1s, (E) Si 2p, and (F) Fe 2p.

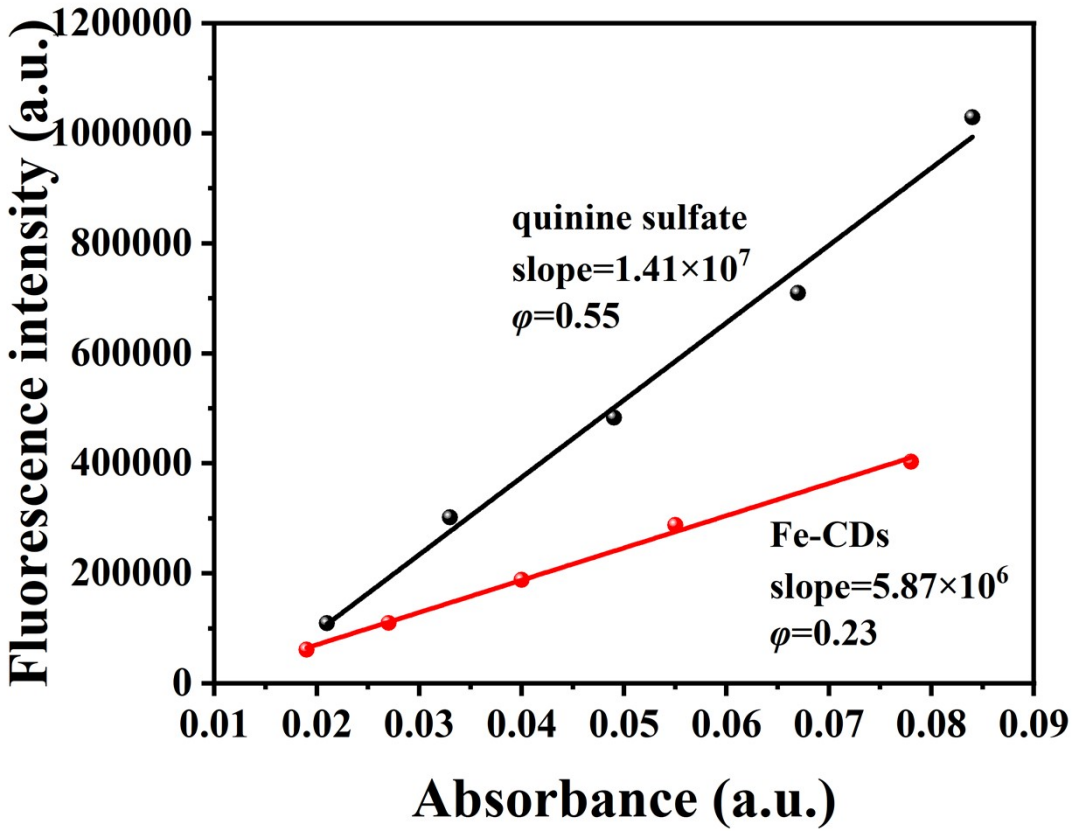

Fig. S3. Relationship between fluorescence intensity and absorbance of Fe-CDs and quinine sulfate under the same excitation wavelength

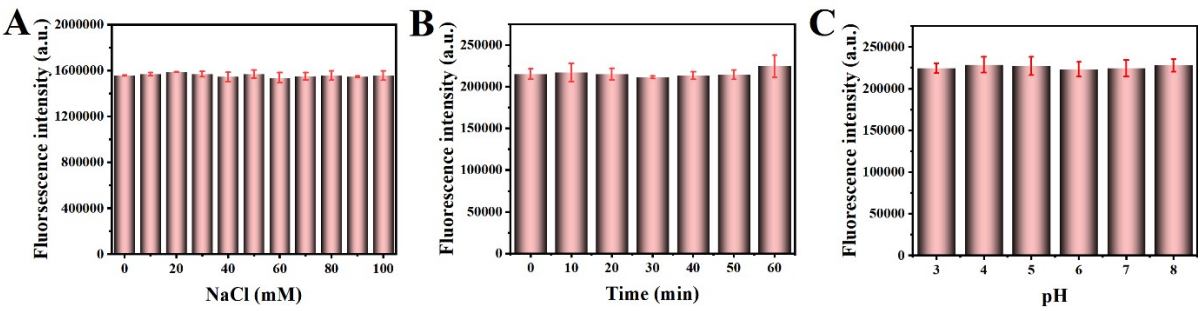

Fig. S4. (A) Effects of ionic strength, (B) UV irradiation time, and (C) pH on the fluorescence intensity of Fe-CDs.

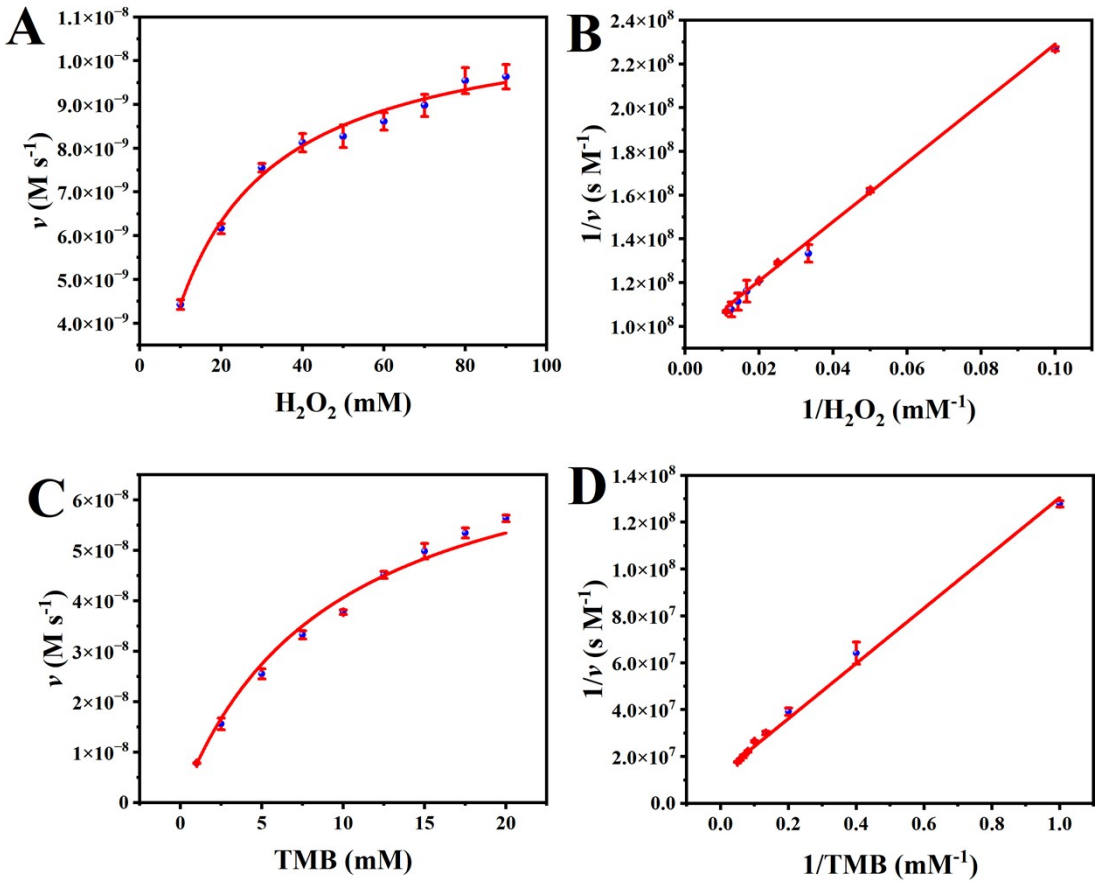

Fig. S5. Steady-state kinetic studies of Fe-CDs for (A) H_2O_2 and (C) TMB; corresponding Lineweaver-Burk double-reciprocal plots for (B) H_2O_2 and (D) TMB.

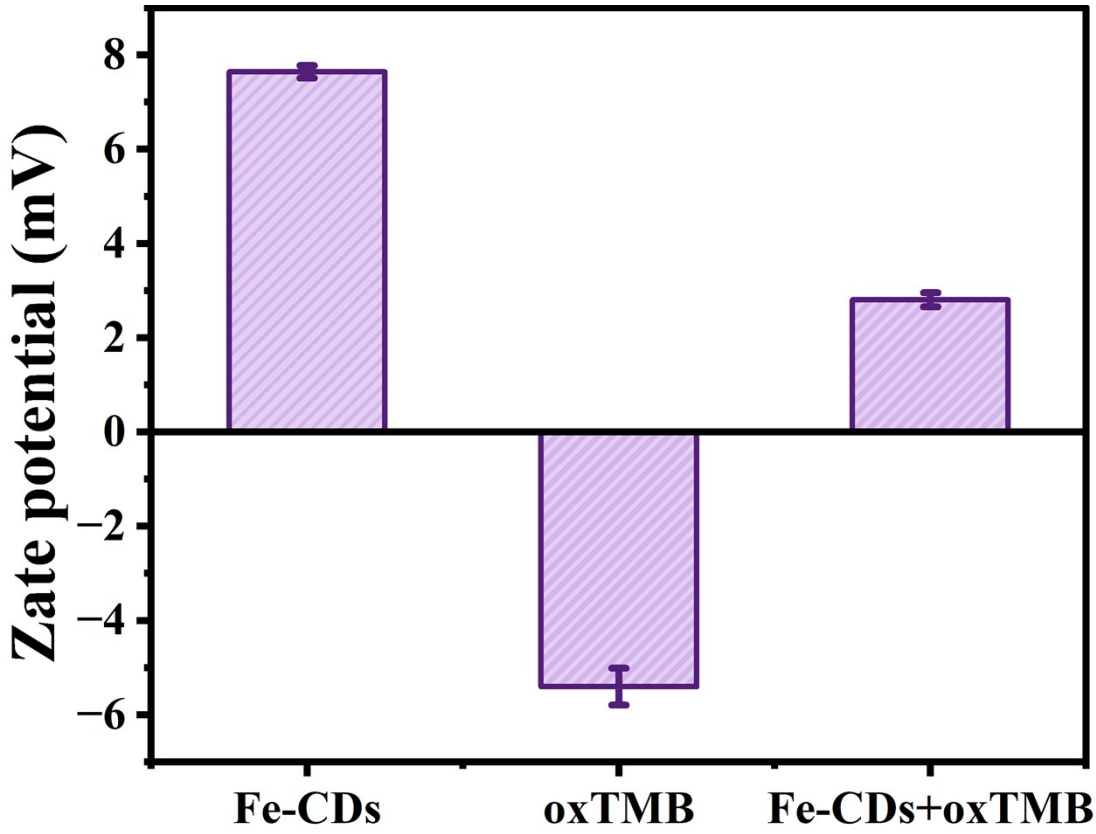

Fig. S6. Zeta potentials of Fe-CDs, oxTMB, and Fe-CDs mixed with oxTMB.

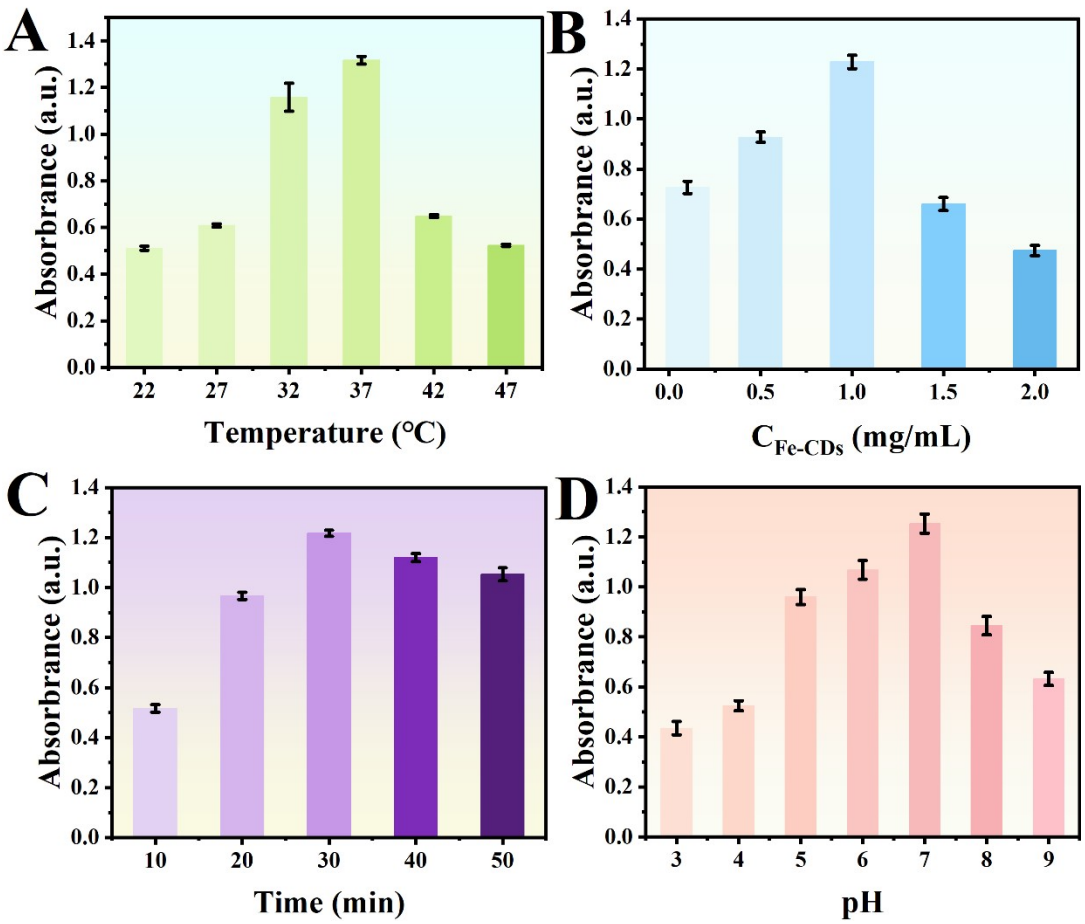

Fig. S7. Effects of reaction conditions on the fluorescence intensity of the sensing system: (A) reaction temperature, (B) Fe-CDs concentration, (C) reaction time, and (D) pH.

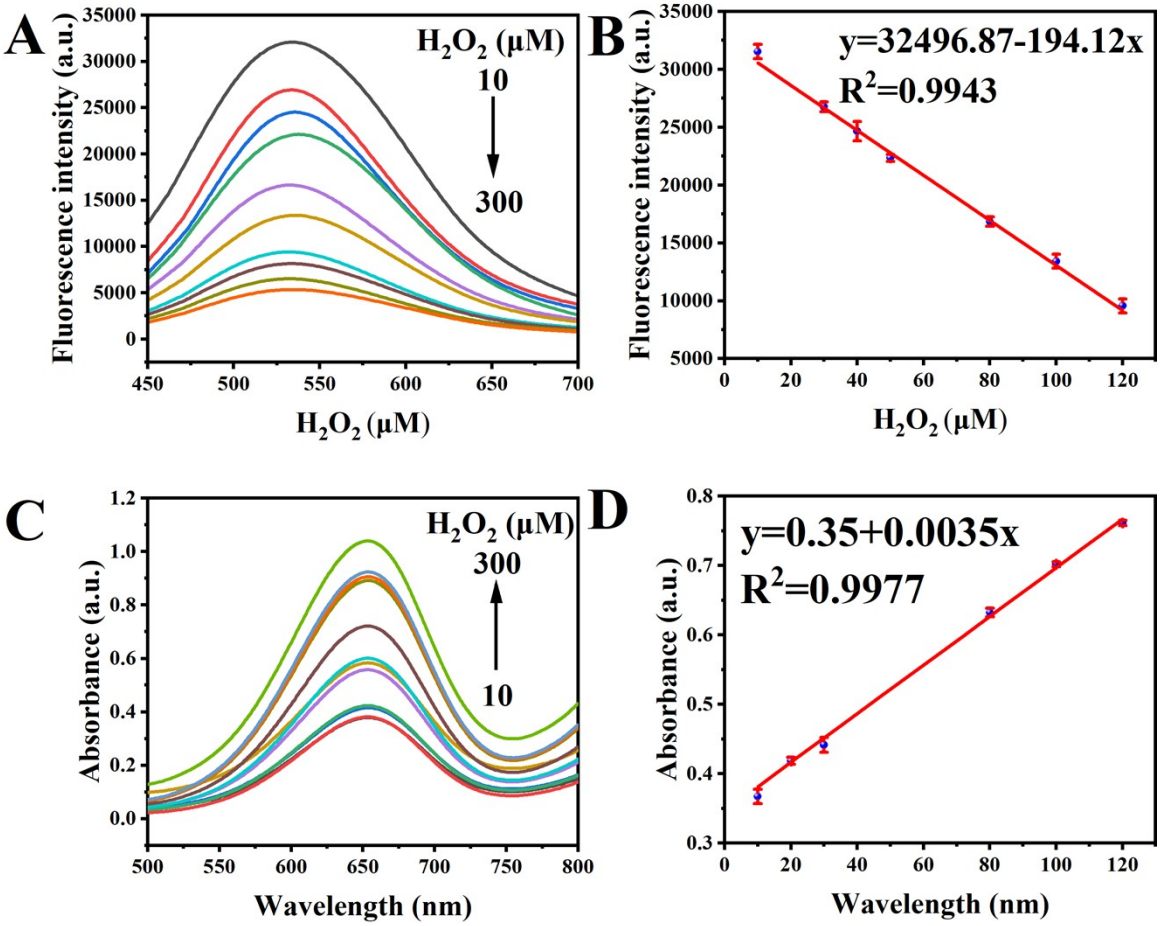

Fig. S8. (A) Fluorescence responses of the Fe-CDs/TMB system upon addition of different concentrations of H_2O_2. (B) Linear relationship between fluorescence intensity and H_2O_2 concentration. (C) Absorbance of the Fe-CDs/TMB system after adding varying levels of H_2O_2. (D) Linear relationship between absorbance intensity and H_2O_2 concentration.

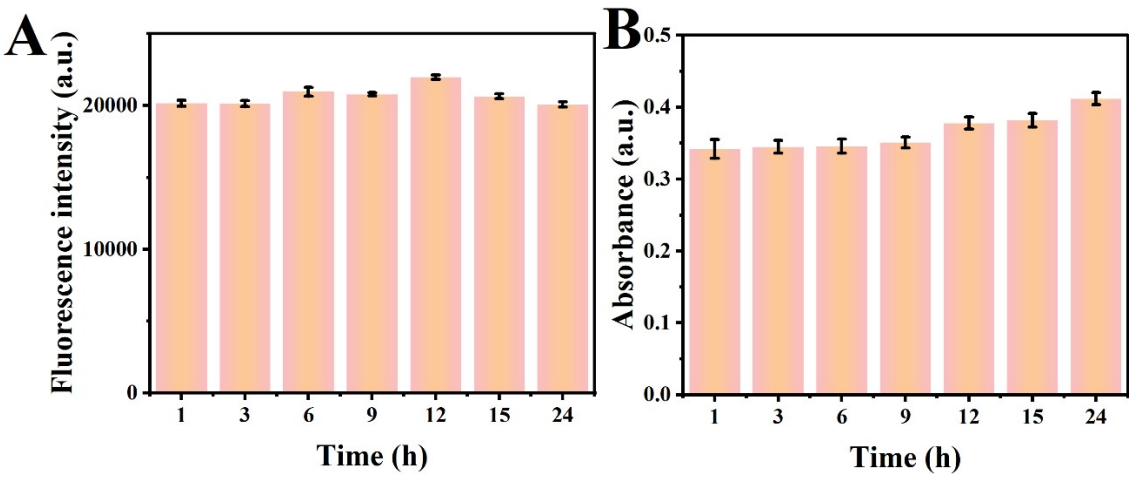

Fig. S9. (A) Fluorescence intensity and (B) UV absorbance of a sample measured at different time points.

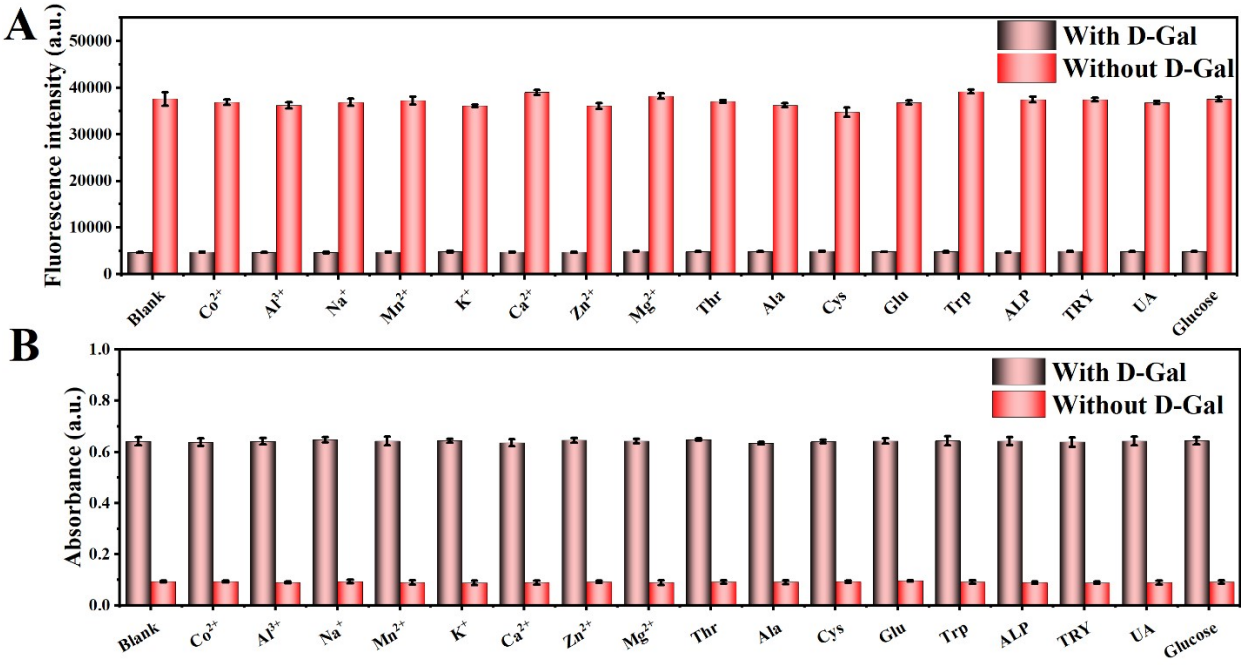

Fig. S10. Effects of different potential interferents on D-Gal detection: (A) fluorescence intensity and (B) UV absorption.

Table S1. Comparison of the kinetic parameters of different peroxidase mimics.

Catalyst	Substrate	K_m（mM）	V_{max}（M/s）	Reference
KCl-LCDs	H_2O_2	0.19	11.63×10^{-8}	S1
	TMB	0.26	2.51×10^{-6}	
HRP	H_2O_2	0.434	8.71×10^{-8}	S2
	TMB	3.70	10.00×10^{-8}	
LS-CDs	H_2O_2	0.32	19.53×10^{-7}	S3
	TMB	0.26	15.62×10^{-7}	
WS_2/rGO	H_2O_2	10.001	0.93×10^{-8}	S4
	TMB	22.406	0.96×10^{-8}	
Cu-BDC@$FeMo_6$	H_2O_2	0.69	7.12×10^{-8}	S5
	TMB	1.81	10.53×10^{-8}	
Cu-NS	H_2O_2	14.3	6.79×10^{-8}	S6
	TMB	0.1	3.89×10^{-8}	
Co@Fe MOG	H_2O_2	0.72	2.87×10^{-8}	S7
	TMB	3.13	10×10^{-8}	
Fe-CDs	H_2O_2	0.443	1.066×10^{-7}	This work
	TMB	0.0932	7.911×10^{-7}	

Table S2. Comparison of analytical methods for the determination of D-Gal

Detection method	Sensing system	Linear range (mM)	LOD (μM)	Ref.
Phosphorimetry	QDs	0.02-0.8	8	[S8]
Electrochemistry	Os-based redox polymers	1-8	39	[S9]
Colorimetry	GAOx@MOF	0.02-1	6.7	[S10]
Fluorimetry	APBA-Cdots	0-0.5	6.2	[S11]
Colorimetry	GeO_2 nanoparticles	0.1-1.5	50	[S12]
Fluorimetry	Fe-CDs	0.001-120	0.25	This work
Colorimetry	Fe-CDs	0.1-100	19	This work

References

S1 X. Y. Xu, Q. J. Sun, Y. M. Ma, X. X. Jiang, N. Niu and L. G. Chen, Synthesis of KCl-doped lignin carbon dots nanoenzymes for colorimetric sensing glutathione in human serum, *Sensor Actuat. B-Chem.*, 2022, **364**, 9, DOI: 10.1016/j.snb.2022.131881.

S2 S. Y. Fu, S. Wang, X. D. Zhang, A. H. Qi, Z. R. Liu, X. Yu, C. F. Chen and L. L. Li, Structural effect of Fe_3O_4 nanoparticles on peroxidase-like activity for cancer therapy, *Colloid Surf. B-Biointerfaces*, 2017, **154**, 239-245, DOI: 10.1016/j.colsurfb.2017.03.038.

S3 C. H. Yin, Q. J. Sun, M. Wu, X. L. Yu, N. Niu and L. G. Chen, Novel lignin-derived carbon dots nanozyme cascade-amplified for ratiometric fluorescence detection of xanthine oxidase and intracellular imaging, *Sens. Actuators, B*, 2024, **406**, 10, DOI: 10.1016/j.snb.2024.135458.

S4 S. Keerthana, A. Rajapriya, C. Viswanathan and N. Ponpandian, Enzyme like-colorimetric sensing of H_2O_2 based on intrinsic peroxidase mimic activity of WS_2 nanosheets anchored reduced graphene oxide, *J. Alloy. Compd.*, 2021, **889**, 11, DOI: 10.1016/j.jallcom.2021.161669.

S5 Y. Xu, J. H. Zhou, P. Sun, P. Li, D. X. Han, X. H. Wang and F. Chai, The construction of peroxidase-like Cu-BDC@$FeMo_6$ for colorimetric detection of H_2O_2 and dopamine, *Sep. Purif. Technol.*, 2025, **353**, 13, DOI: 10.1016/j.seppur.2024.128396.

S6 X. P. Yang, X. Y. Xie, L. Jiang, Y. X. Fan, C. L. Zhang and Y. Wang, Cu-NC single-

atom nanozymes with peroxidase-like activity for colorimetric detection of D-penicillamine, *Talanta*, 2025, **283**, 8, DOI: 10.1016/j.talanta.2024.127131.

S7 M. Wang, X. G. Zhu, Y. N. Yin, G. X. Ling and P. Zhang, Porous reticular Co@Fe metal-organic gel: dual-function simulated peroxidase nanozyme for both colorimetric sensing and antibacterial applications, *J. Mat. Chem. B*, 2024, **12**, 5418-5430, DOI: 10.1039/d4tb00446a.

S8 J. Z. Lv, W. L. Yang and Y. M. Miao, Preparation of galactose oxidase functional phosphorescent quantum dots and detection of D-galactose, *Spectroc. Acta Pt. A-Molec. Biomolec. Spectr.*, 2020, **240**, 8, DOI: 10.1016/j.saa.2020.118599.

S9 C. Figueiredo, A. García-Ortega, T. Mandal, A. Lielpetere, F. Cervantes, D. Demurtas, E. Magner, F. J. Plou, W. Schuhmann, D. Leech, M. Pita and A. L. De Lacey, An oxygen-insensitive amperometric galactose biosensor based on galactose oxidase co-immobilized with an Os-complex modified redox polymer, *Electrochim. Acta*, 2023, **472**, 8, DOI: 10.1016/j.electacta.2023.143438.

S10 H. Huang, D. H. Song, W. J. Zhang, Y. Sun and Y. X. Li, One step cascade detection of galactose based on a galactose oxidase-composited peroxidase nanozyme, *Anal. Methods*, 2022, **14**, 3644-3651, DOI: 10.1039/d2ay01224c.

S11 J. A. Yang, X. W. He, L. X. Chen and Y. K. Zhang, The selective detection of galactose based on boronic acid functionalized fluorescent carbon dots, *Anal. Methods*, 2016, **8**, 8345-8351, DOI: 10.1039/c6ay02530g.

S12 P. T. Nguyen, H. T. Ahn and M. I. Kim, Reagent-free colorimetric assay for galactose using agarose gel entrapping nanoceria and galactose oxidase,

Nanomaterials, 2020, **10**, 10, DOI: 10.3390/nano10050895.